From the Research of Contract Beamline
～BL12B2/12XU（NSRRC）～

Developed *in-situ* X-ray Spectroscopy to Investigate the Catalyst System toward Oxygen Evolution Reaction

Chia-Shuo Hsu and Hao Ming Chen*

Department of Chemistry, National Taiwan University, Taipei 106, Taiwan

Abstract

Oxygen evolution reaction (OER) is a half reaction of water splitting. Toward this end, transition-metal oxides have been demonstrated to act as electrocatalysts for OER. Among various transition-metal oxides, *3d* transition metals with spinel structures were widely used for being active electrocatalysts toward this reaction. Nevertheless, spinel is a complex structure, in which two oxidation state of metal ions as well as two different crystallographic sites are present in this structure. To investigate the behavior of spinel structure during OER, we have developed both *in-situ* X-ray absorption spectroscopy and *in-situ* grazing-angle X-ray diffraction manner, while various well-designed samples were prepared to figure out the dominated factors step by step. First, we have modified the electrocatalysts with surface reversibly adapting layer to improve the resulting stability. Second, we choose the spinel structure with bimetallic system of $NiCo_2O_4$ to reveal the active cite between these two metals. Furthermore, the non-active metals were employed to substitute for the divalent and trivalent metal ions in spinel to point out the active centers. The effects of crystallographic sites were verified by a model system of inverse spinel Fe_3O_4 with replacing by Co, Ni, and Zn divalent metal ions. As a result, we can clarify that the divalent metal ions are the active center for OER in the spinel structure, while a phase transformation to metal oxyhydroxide which act as the real active phase is needed to achieve a higher performance. From the result of understanding spinel behavior toward OER, we can realize that the *in-situ* X-ray spectroscopy is a useful technique, and believed that this technique can be used not only in spinel structure but other catalyst for other reactions.

Introduction

People have relied on carbon-based fuel to produce electricity for many year, but these carbon-based fuels will run out within years[1]. On the other hand, carbon dioxide which is a main factor for inducing the greenhouse effect is a by-product during burning of carbon-based fuel[2]. Therefore, finding renewable sources to replace fossil fuel has become the most imperative thing. There are various alternatives to approach this goal such as solar energy, hydrogen through solar water-splitting, tidal energy, and wind power. Among these renewable energy, solar water-splitting is highly desired direction because its high efficiency to convert solar energy into hydrogen gas and oxygen gas[3-5].

Water splitting reaction is combined by two half reactions including the hydrogen evolution reaction (HER, $2H_2O + 2e^-$ $\rightarrow H_2 + 2OH^-$) and the oxygen evolution reaction (OER, $2H_2O$ $\rightarrow O_2 + 4e^- + 4H^+$)[6]. Although only hydrogen gas generated at the cathode is energy storage substance, oxygen gas generated at the anode still need to be remarkably considered.

Because OER is the kinetic barrier for driving water splitting reaction, which contains a four-electron transfer process while HER involves a two-electron transfer[7]. Accordingly, the OER requires a higher overpotential to overcome the kinetic barrier for completing the oxygen evolution. In recent years, variety of metal oxides were used as electrocatalysts for OER. Among these catalysts, RuO_2 and IrO_2 can performe the lowest overpotentials
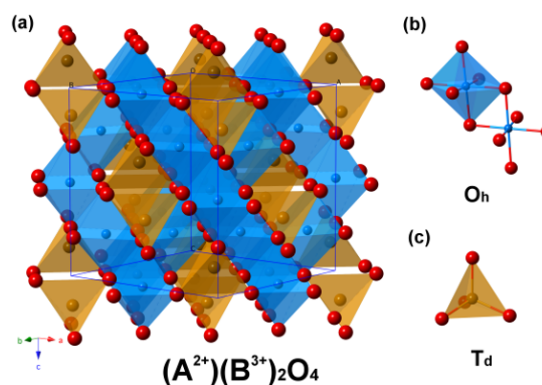

Figure 1 Crystal structure of inverse spinel AB_2O_4 and corresponding octahedral site (O_h) and tetrahedral site (T_d).
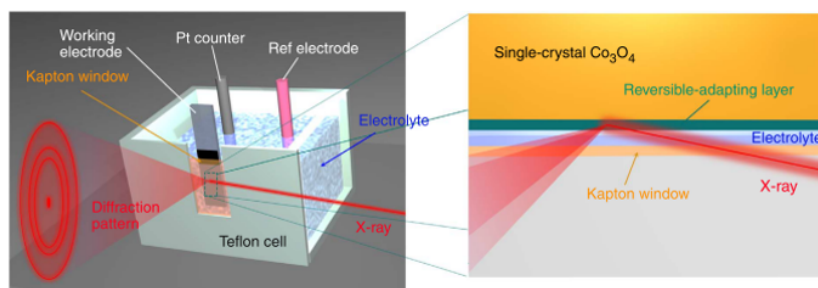
Figure 2　Schematic representation of the *in-situ* grazing-angle X-ray diffraction apparatus applied to a liquid electrochemical cell.

with the values of 0.36 V and 0.4 V and showed Tafel slopes of 55 and 91 mV/dec, respectively[8]. However, these two oxides are made of precious metals and unstable in the alkaline condition. As a consequence, many research groups are developing the earth-abundant materials with *3d* transition metal oxides to achieve the goals of both stability and activity toward the OER[9,10].

Within *3d* transition metal oxides, spinel-type metal oxides have exhibited highly potential toward OER due to its high conductivity and stability in alkaline condition. The spinel with a formula of AB_2O_4[11] is a complex system, where one divalent (A^{2+}) metal ions and the other two metals with trivalent (B^{3+}) character are present. A and B atoms can be group 2, group 13, and first-row transition metals, while two crystallographic site, octahedral (O_h) and tetrahedral (T_d) sites, are in this structure (Figure 1). Moreover, there are two possible combinations, in which one is normal spinel $(A^{2+}_{Td})(B^{3+}_{Oh})_2O_4$ (divalent cation A^{2+} in tetrahedral site) and the other one is inversed spinel $(A^{2+}_{Oh})(B^{3+}_{Td})(B^{3+}_{Oh})O_4$ (divalent cation A^{2+} in octahedral site). With the aim of realizing the key factors for active electrocatalysts toward OER in spinel system, it's essential to significantly consider both chemically oxidation state (divalent and trivalent) and two crystallographic sites in the structure. For these reasons, it's great challenge to recognize the role of metal ions upon the activity toward OER in spinel system.

Zhang *et al*. have used an *in-situ* FTIR (Fourier-Transform Infrared Spectrometer) experiment to reveal that -OOH group would be formed on the surface of spinel Co_3O_4 during OER[12]. It has pointed out a fact that the surface condition is much different from that of inner part of catalyst. And the surface should be a key toward the activity during OER[13]. Additionally, the -OOH group can be observed only during the reaction undergoing. Thus, it is necessary to develop an *in-situ* technique for fully understanding how the electrocatalysts work during the reaction.

Methodology

Since X-ray technique is a powerful method for characterizing the nature of materials. We designed a liquid cell made of Teflon for collecting the X-ray elastic/inelastic scattering with applying a voltage at the same time. A liquid cell as show in Figure 2 was designed for *in-situ* X-ray absorption spectroscopy (XAS). The X-ray-light source aimed at the working electrode, and the Lytle detector was collect the fluorescence signal at the location of 90 degrees. It is really a useful method to characterize the nature of materials by XAS. By utilizing the *in-situ* set up, it will become more helpful to realize the alternative of oxidation states and the change of the coordination shell. In the case of *in-situ* X-ray diffraction, we created a window on the liquid cell to collect the diffraction patterns by using a Kapton tap to prevent the liquid from flowing out, in which a three-electrode system is performed for electrochemical testing and the FTO (Fluorine-doped Tin Oxide) acts as substrate of work electrode. Because the reaction should occur at the interface between the electrocatalysts and electrolyte, more information can be obtained at the top of side which load samples. Otherwise, it's well-known that the reactions
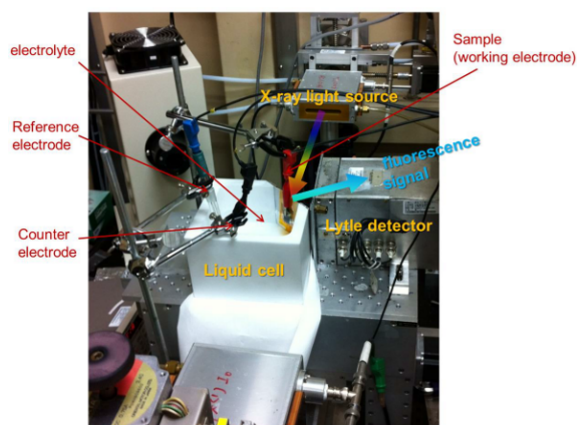

Figure 3　Digital photograph of a hand-made chemical cell for use *in-situ* X-ray absorption measurement.

happened only on the surface of electrocatalyst, we utilized a grazing-angle X-ray diffraction to maximize the contribution from the surface of electrocatalysts (as shown in Figure 3)[14]. Both *in-situ* X-ray absorption and X-ray diffraction experiments were collected at BL12B2, and recently we also conducted this set up at BL12XU of SPring-8.

Result

In first case, we designed single crystal Co_3O_4 nanocubes to investigate the behavior during OER. Single crystal can significantly rule out the influence of defects and avoid self-oxidizing. Furthermore, we reduced the surface Co_3O_4 into CoO with sodium borohydride ($Co_3O_4@CoO$)[14] because of a higher activity of rock salt CoO than that of spinel during the OER[15]. In terms of the electrochemical performance, metal oxides were tested by linear scanning voltammetry (LSV) with corresponding Tafel plots. $Co_3O_4@CoO$ sample shown a comparable performance as compared to that of RuO_2 and IrO_2 that performed low overpotentials as we mentioned above. The activity of OER usually compares at a current density of $10\,mA/cm^{-2}$,
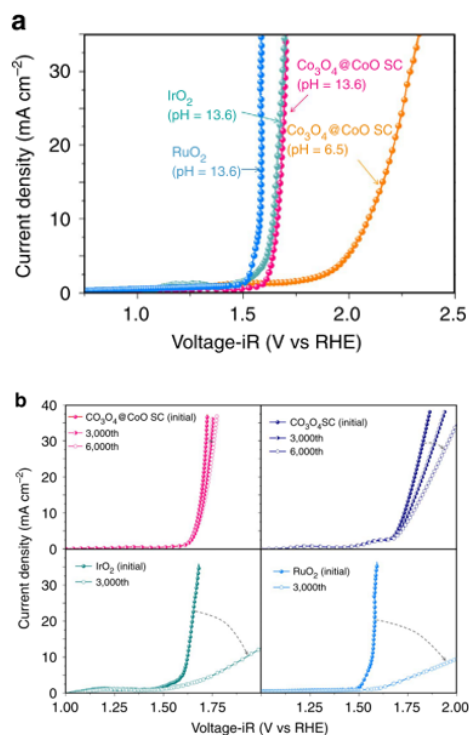

Figure 4 (a) LSV curves of $Co_3O_4@CoO$ in alkaline (0.5 M KOH; pH = 13.6) and neutral (0.5 M Na_2SO_4; pH = 6.5) conditions, commercial RuO_2 catalysts (0.5 M KOH; pH = 13.6), and IrO_2 catalysts (0.5 M KOH; pH = 13.6). (b) LSV curves of $Co_3O_4@CoO$, Co_3O_4, IrO_2, and RuO_2 catalysts subjected to continual potential cycling between 1.0 and 2.0 V (versus RHE) in 0.5 M KOH for 3,000 (and 6,000) cycle measurements.

because this value represented a 10% efficiency of solar-to-fuel conversion. $Co_3O_4@CoO$ samples reached this current density at 0.430 V, while RuO_2 and IrO_2 with the value of 0.411 V and 0.358 V, respectively. It showed that $Co_3O_4@CoO$ sample performed almost the same value to these two catalyst. Although the Tafel slope of $Co_3O_4@CoO$ sample is not the lowest one among *3d* transition metal oxides, it can also present high activity at neutral condition, as show in Figure 4.

For the *in-situ* XAS experiment result (Figure 5), we can observe several coordination shells in $Co_3O_4@CoO$ sample. In the low potential we applied (below +1.7 V versus RHE; Reversible Hydrogen Electrode), three shells can be obtained in the extended X-ray absorption fine structure spectra (EXAFS). First shell appeared at ~ 1.5 Å, second and third shells were at ~ 2.5 and 3.1 Å, respectively. For the spinel structure, the first shell is the scattering with the closet oxygen (Co-O), the second and third ones are both the scattering with two cobalt (Co-Co). The second shell with the Co-Co distance at ~ 2.5 Å can be referred to Co(III)-Co bond with octahedrally coordinated Co atoms in a normal spinel structure. The third shell represented Co(II)-Co bonds with tetrahedrally coordinated Co atoms. However, the most interesting thing was at ~ 3.8 Å once we applied higher potential (over +1.7 V versus RHE). There is a new peak can be observed, this peak could be a new Co-O scattering path which can be attributed to the formation of cobalt oxyhydroxide. Thus, we can suggest that the CoO on the surface of Co_3O_4 should transfer to cobalt oxyhydroxide during OER.

The result of *in-situ* grazing-angle X-ray diffraction (Figure 6) showed that the characteristic peaks of spinel structure, and no CoO phase can be observed. Once we applied higher voltage, we can notice that the β-CoOOH formed at the lower
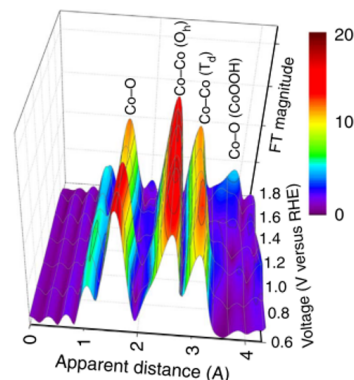

Figure 5 Voltage-dependence Fourier transform extended X-ray absorption fine structure spectra of a $Co_3O_4@CoO$ in an alkaline aqueous solution containing 0.5 M KOH (pH = 13.6) and in an *in-situ* liquid cell.

angle ($Q = 1.4$ Å^{-1})[16]. Once a higher voltage was applied, another phase, α-CoOOH, would also generate. Apparently, this behavior happened both in alkaline and neutral environments. This is the first direct evidence to prove the formation of metal oxyhydroxide during oxygen evolution. To combine with results of XAS, we can confirm that the CoO layer on the surface would transfer into an active phase (metal oxyhydroxide). Furthermore, in the case of a cycled potential between +2 V and +0.1 V versus RHE, metal oxyhydroxide,

the active phase, appeared at high voltage and disappear at low voltage (Figure 6b). It was worth to find that metal oxyhydroxide would produce again when the voltage increased to the higher one, which referred to a fact that the CoO layer as a junction layer that could alter this structure reversibly between amorphous and metal oxyhydroxide. Due to the presence of this junction layer, it can protect the inner structure and adapt to the environment with bias for providing a more stable electrocatalyst for oxygen evolution reaction[14].
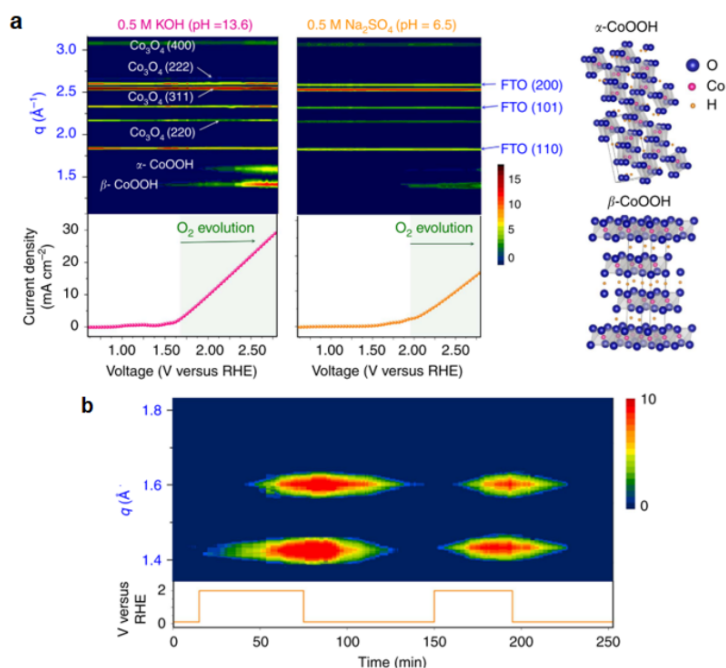

Figure 6　(a) Contour plots of *in-situ* grazing-angle X-ray diffraction signals of a Co$_3$O$_4$@CoO in an aqueous solution containing 0.5 M KOH (pH = 13.6) and 0.5 M Na$_2$SO$_4$ (pH = 6.5). The images show the diffraction intensity (colour coded) as a function of voltage, and data collection was performed at the NSRRC synchrotron facility by using 12 keV of energy. The lower curves show the measured current density in both cases. (b) Contour plots of *in-situ* grazing-angle X-ray diffraction signals of a Co$_3$O$_4$@CoO in an alkaline aqueous solution under switching of voltage (between 2.0 and 0.1 V versus RHE), and data collection was performed at the synchrotron facility by using 10 keV of energy to achieve better position distinguishability.
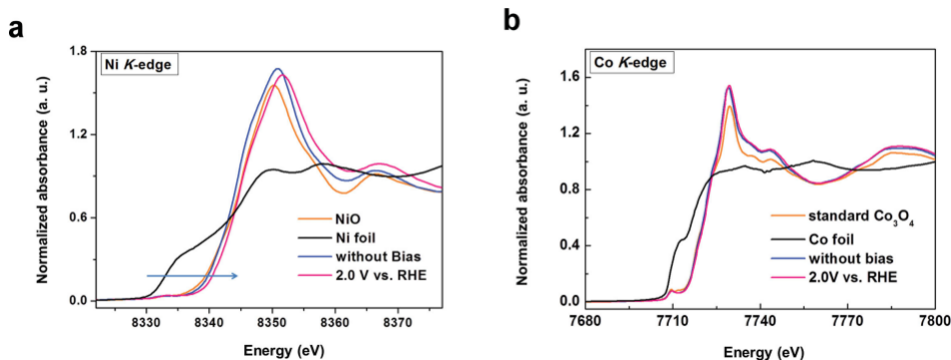

Figure 7　Normalized *in-situ* (a) Ni K-edge and (b) Co K-edge XANES spectra for NiCo$_2$O$_4$ electrode with and without applied bias in 1 M NaOH.
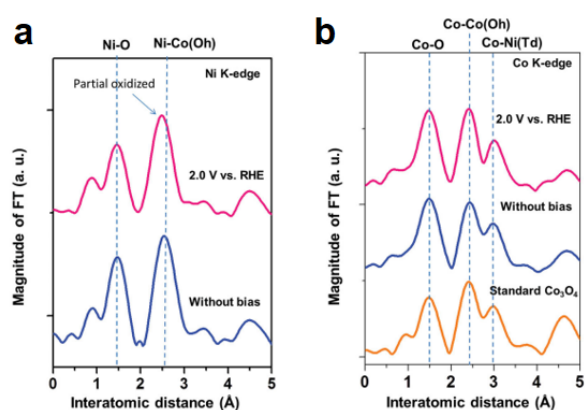
Figure 8   EXAFS oscillations extracted from *in-situ* (a) Ni K-edge and (b) Co K-edge EXAFS spectra for $NiCo_2O_4$ with and without applied bias in 1 M NaOH.

As we mentioned above, the spinel system is a complex system, where both $Co_3O_4@CoO$ and Co_3O_4 are metal oxides with single metal element. It will be necessary to design the electrocatalysts that can individually study the roles of metal ions. According this, we introduced nickel ions into spinel structure to obtain the $NiCo_2O_4$ for investigating the active site of spinel structure. Nickel(II) is the most stable state in common metal oxides, so it can substitute for the Co(II) in the Co_3O_4 structure while the NiO is also a good electrocatalyst for OER[17]. $NiCo_2O_4$ is a normal spinel structure, which means that Ni located at tetrahedral site of spinel structure. In this case, the individual role of metal ions can be much easier clarified the factor toward OER between two metal ions. As a consequence, to realize the active site in $NiCo_2O_4$ structure, *in-situ* XAS is a good manner to achieve the goal that individually investigate the behaviors of Co and Ni ions through studying the corresponding X-ray absorption spectra. For the result of *in-situ* X-ray absorption near edge structure (XANES), the spectra of Ni K-edge changed with increasing the applied potential in 1

M NaOH (Figure 7). Initially, the energy position of absorption-edge is located in 8,350.2 eV. After increasing the applied voltage, the energy shifted to a higher value of 8,350.7 eV with continuously decreasing the intensity of white line. It indicated that the oxidation state increased during OER, and this increase in oxidation state could be referred to the formation of NiOOH. On the other hand, the energy position of Co K-edge presented a constant value ($\sim$ 7,729.3 eV) as illustrated in Figure 7b during the water oxidation. It suggested that the environment of Co ions did not change during the reaction. For EXAFS spectra of Ni ions (Figure 8), the first path is the Ni-O scattering path, and the distance of Ni-O path is around 1.5 Å. The second path with the distance of 2.5 Å is the Ni-Co(O_h) scattering. Notably, the second path decreased once the bias was applied. It could be the oxidation from Ni^{2+} to Ni^{3+}, which led to a decrease in the radii of Ni ions. Besides, the EXAFS spectra of Co ions showed three paths at 1.5 Å, 2.5 Å, and 3.0 Å. Three paths could be attributed to the Co-O, Co-Co(O_h), and Co-Ni(T_d), respectively. The only path that referred to Ni ions has changed as showed in Figure 8b. Consequently, the Ni ions might be the active site in $NiCo_2O_4$, while the Co ions in this structure seem to be the minor roles toward the catalytic reaction. Thus, we can realize that various metal atoms might act as different roles during OER. But there is still something unclear, it need to confirm that either the structural site or the oxidation state dominate the activity of OER[18].

To recognize the influence from oxidation state, both Zn(II) and Al(III) ions that were well-known as non-active metal ions for OER were employed to replace the Co(II) and the Co(III) in Co_3O_4, respectively. For the activity of OER, cobalt oxide and substituted cobalt oxides were tested by both cyclic voltammetry (CV) and to obtain the Tafel plots. CV curves showed that the activity of $CoAl_2O_4$ was similar to that of Co_3O_4
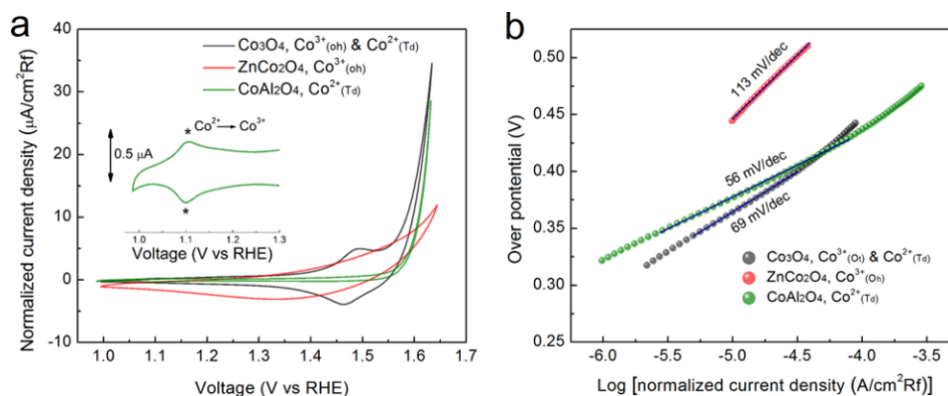

Figure 9   Electrochemical performance toward OER. (a) Cycling voltammetry curves and (b) corresponding Tafel slopes for Co_3O_4, $ZnCo_2O_4$, and $CoAl_2O_4$.

and ZnCo$_2$O$_4$ was much different from the others (Figure 9a). This behavior also performed a similar trend in Tafel slope. The Tafel value of ZnCo$_2$O$_4$ was 113 mV/dec which was higher than that of both CoAl$_2$O$_4$ and Co$_3$O$_4$ (around 60 mV/dec). The result from electrochemistry indicated that the metal ions with oxidation state of +2 were going to dominate the performance. CoAl$_2$O$_4$ containing Co(II) can perform a higher activity as compared with ZnCo$_2$O$_4$ and was similar to that of Co$_3$O$_4$. In contract, ZnCo$_2$O$_4$ lacks of Co(II) and leads to a lower activity than the others. Additionally, the *in-situ* XAS clarified a similar trend to the observations from electrochemistry. The first difference recognized from EXAFS spectra was only two

coordination shells in CoAl$_2$O$_4$ while there are three coordination shells in both ZnAl$_2$O$_4$ and Co$_3$O$_4$ (Figure 10a-c). The first shell with a distance of 1.5 Å should be the Co-O scattering path, and the second path (2.5 Å) which CoAl$_2$O$_4$ sample lacked was the scattering path of Co-Co(O$_h$). The last one was the paths of Co-Co(T$_d$), Co-Zn(T$_d$), and Co(T$_d$)-Al. It verified that all of these samples were normal spinel, wherethe metal ions with oxidation state of +2 occupied the tetrahedral site in the structure. Once the voltage was applied, the first shell of both CoAl$_2$O$_4$ and Co$_3$O$_4$ that contained Co(II) ions has changed while the ZnCo$_2$O$_4$ stayed in the same place during the reaction (Figure 10d). The XANES also reveal a different
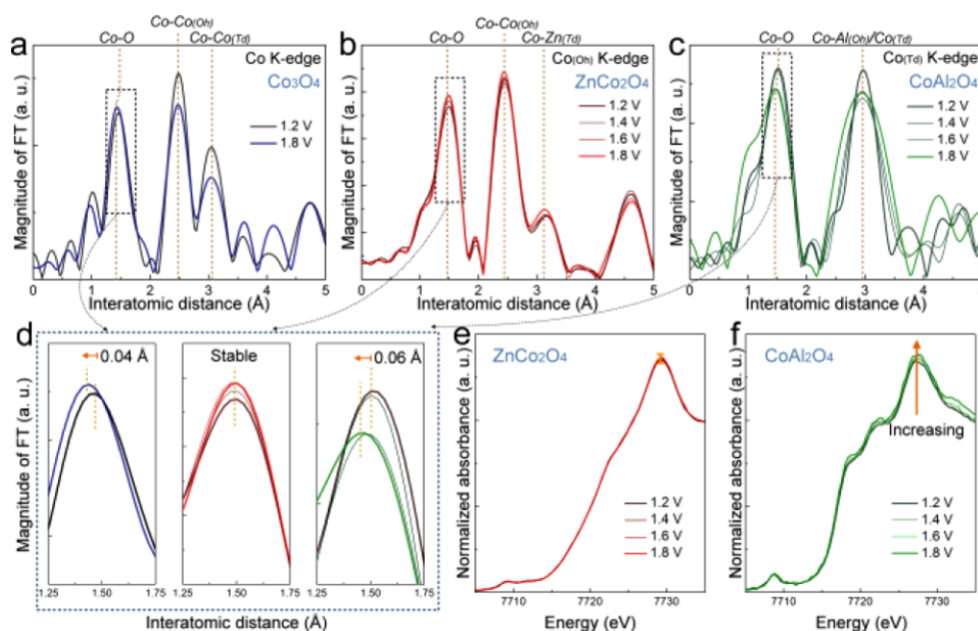

Figure 10   *In-situ* X-ray absorption spectroscopy. (a–c) Co K-edge EXAFS spectra for Co$_3$O$_4$, ZnCo$_2$O$_4$, and CoAl$_2$O$_4$, where the applied voltage is referenced to RHE. (d) Enlarged Co K-edge EXAFS spectra Co–O interatomic distance for Co$_3$O$_4$ (blue), ZnCo$_2$O$_4$ (red), and CoAl$_2$O$_4$ (green). (e and f) Normalized in operando Co K-edge XANES spectra for ZnCo$_2$O$_4$ and CoAl$_2$O$_4$.
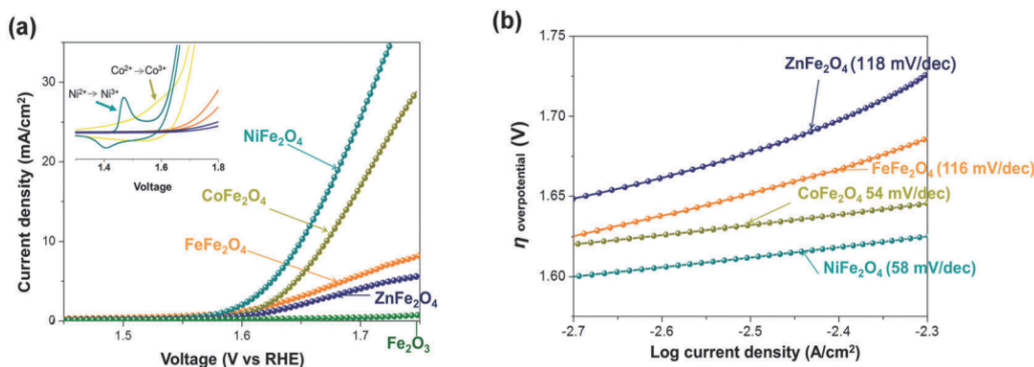

Figure 11   Electrochemical performance and gas evolution for a series sample of MFe$_2$O$_4$ (M = Fe, Co, Ni, Zn). (a) LSV curves were performed in alkaline electrolyte (0.5 M KOH). Insert: Cyclic voltammogram of each sample. (b) Steady-state Tafel (overpotential vs log current) measurements in alkaline electrolyte (0.5 M KOH).
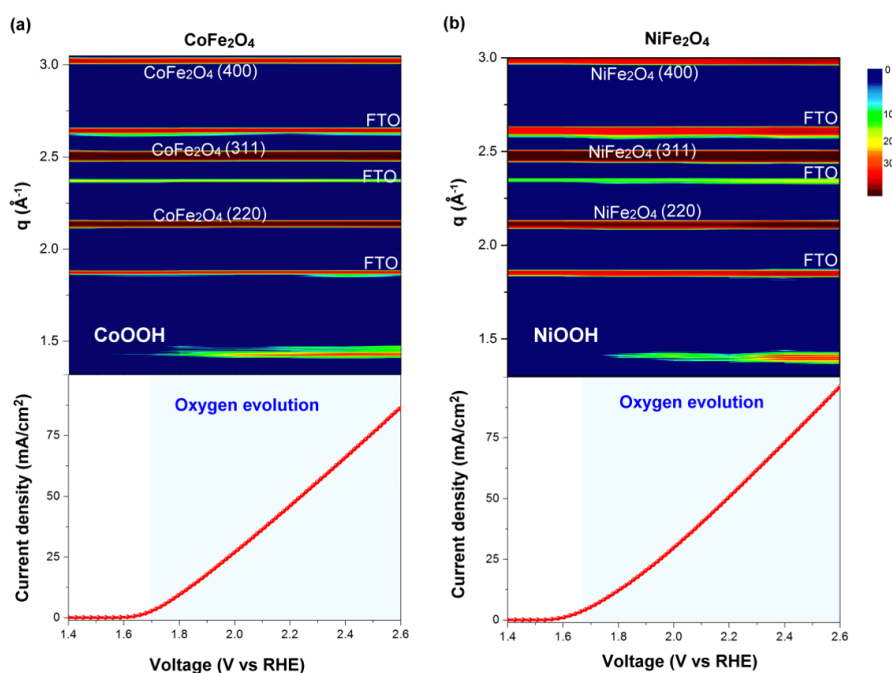
Figure 12　Contour plots of *in-situ* grazing angle X-ray diffraction signals of $CoFe_2O_4$ and $NiFe_2O_4$ samples in an aqueous solution containing 0.5 M KOH, and corresponding measured current density as function of applied voltage in both cases. The images show the diffraction intensity (color-coded) as a function of voltage, and data collection was performed by using 12 KeV of energy.
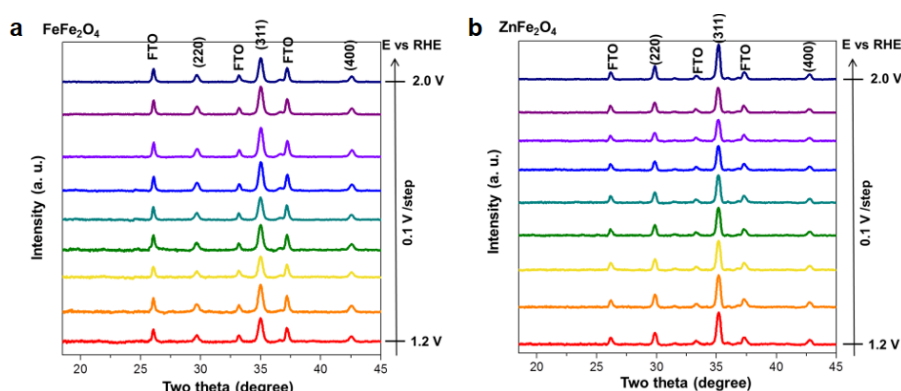

Figure 13　*In-situ* XRD spectra of (a) $FeFe_2O_4$ (b) $ZnFe_2O_4$ samples, a KOH electrolyte of 0.5 M was employed and all measurements with a potential range from 1.2 to 2.0 V vs RHE were operated potentiostatically.

behavior between $ZnCo_2O_4$ and $CoAl_2O_4$ samples (Figure 10e and f). The white line intensity of $CoAl_2O_4$ sample would change when voltage was applied. As mentioned above, the peak shift could refer to the oxidization of metal. The Co(II) within both $CoAl_2O_4$ and Co_3O_4 samples would form CoOOH. That's the reason why a higher performance of $CoAl_2O_4$ and Co_3O_4 than that of $ZnCo_2O_4$. As a result, the active site in the spinel structure can be clarified as the divalent metal ions. The divalent metal of $CoAl_2O_4$ and Co_3O_4 was Co(II), while the divalent metal ions of $ZnCo_2O_4$ was Zn(II) that has been reveal to be inactive for OER[19].

On the other hand, the effects of different crystallographic sites need to be further confirmed. Toward this end, Fe_3O_4 with an inverse spinel structure has been utilized as a model system. The electronic configuration of iron is d^5, and the energy difference is small between octahedral site and tetrahedral site. So the iron ions can possibly occupy both two sites. Based on the crystal-field theory and linear muffin tin orbital (LMTO) calculation, most of the divalent M^{2+} ions prefer occupying octahedral sites rather than tetrahedral positions[20]. Co, Ni, and Zn ions substituted for the divalent metal ions in the Fe_3O_4. For the electrochemical result, LSV results showed that both

CoFe$_2$O$_4$ and NiFe$_2$O$_4$ have a higher performance than the others (Figure 11a). The oxidation peak can be only observed in CoFe$_2$O$_4$ and NiFe$_2$O$_4$ samples (Figure 11a, insert), while Tafel slope can separate into two groups, CoFe$_2$O$_4$ and NiFe$_2$O$_4$ were the first group with the value around 55 mV/dec, Fe$_3$O$_4$ and ZnFe$_2$O$_4$ were the second group with a value around 115 mV/dec (Figure 11b).

Therefore, it seemed that the divalent metal is still the active site for OER, while the crystallographic sites should be the minor effect toward the performance. However, the divalent metal ions were placed at the different environments in the structure, indicating that the behavior would be different in the normal spinel structure. Furthermore, *in-situ* grazing-angle X-ray diffraction was used to figure out this issue. When the OER is beginning, both CoFe$_2$O$_4$ and NiFe$_2$O$_4$ exhibited a new peak at Q = 1.4 Å^{-1} with increasing the applied voltage (Figure 12), indicating that the formation of metal oxyhydroxide was a similar behavior to that of Co$_3$O$_4$[21]. In contract to these two samples, Fe$_3$O$_4$ and ZnFe$_2$O$_4$ lacked of any new feature peak or any shift in position at higher voltage (Figure 13), which can explicate the different behavior from the electrochemical observation. The CV curves reveal the oxidation peaks should be referred to the phase transformation into metal oxyhydroxide, and the observations from Tafel slope suggested that the activity of electrocatalysts should refer to this structural transformation. As a result, the occurrence of present structural transformation toward metal oxyhydroxide is the key to dominate the activity of OER. In the cases of both CoFe$_2$O$_4$ and NiFe$_2$O$_4$, the divalent metal ions onto the surface will transform into metal oxyhydroxide, and then the metal oxyhydroxide on the surface will act as the main active phase for OER[22].

Conclusion

In summary, we have provided several systems to understand the operating of spinel structure metal oxides during OER, and have demonstrated the *in-situ* XAS and *in-situ* grazing-angle X-ray diffraction to achieve this goal. First, CoO-modified Co$_3$O$_4$ with reversible junction layer results in a fact that the phase transformation becomes easier and make the electrocatalysts more stable. Second, NiCo$_2$O$_4$ was utilized as a model to realize the active site within the structure for bimetallic spinel oxide, in which Ni is the main active center while Co might not contribute to the reaction. For the influence upon the oxidation state of electrocatalysts toward OER, two metal ions, Zn and Al, well-known as non-active metal for OER were

employed to substitute for the different oxidation states (i.e., Co^{2+} and Co^{3+}) in spinel structure. The result can reveal that the divalent metal ions are the active metal. For the effect of crystallographic site, we choose Fe$_3$O$_4$ with inverse spinel system as a model to address this issue, in which the replacement of the Fe(II) with a series of divalent metal ions to clarify the activities at octahedral site. At the end, we can further confirm that the divalent metal ion is the active site regardless of crystallographic sites. The most importantly, to achieve the excellent activity toward OER, the divalent metal ion has to be transformed into metal oxyhydroxide that is the active phase for OER.

References

[1] Rogner, H. H.: *Annu. Rev. Energy Environ.* **22** (1997) 217-262.

[2] Bert, G. D. a.; Miquel, A. G.-M.; Steve, P. L.: *Annu. Rev. Plant Physiol. Plant Mol. Biol.* **48** (1997) 609-639.

[3] Khan, S. U. M.; Al-Shahry, M.; Ingler, W. B.: *Science* **297** (2002) 2243-2245.

[4] Kudo, A.; Miseki, Y.: *Chem. Soc. Rev.* **38** (2009) 253-278.

[5] Bard, A. J.; Fox, M. A.: *Acc. Chem. Res.* **28** (1995) 141-145.

[6] Walter, M. G.; Warren, E. L.; McKone, J. R.; Boettcher, S. W.; Mi, Q.; Santori, E. A.; Lewis, N. S.: *Chem. Rev.* **110** (2010) 6446-6473.

[7] Suen, N. T.; Hung, S. F.; Quan, Q.; Zhang, N.; Xu, Y. J.; Chen, H. M.: *Chem. Soc. Rev.* **46** (2017) 337-365.

[8] Lee, Y.; Suntivich, J.; May, K. J.; Perry, E. E.; Shao-Horn, Y.: *J. Phys. Chem. Lett.* **3** (2012) 399-404.

[9] McCrory, C. C. L.; Jung, S.; Peters, J. C.; Jaramillo, T. F.: *J. Am. Chem. Soc.* **135** (2013) 16977-16987.

[10] Suntivich, J.; May, K. J.; Gasteiger, H. A.; Goodenough, J. B.; Shao-Horn, Y.: *Science* **334** (2011) 1383-1385.

[11] Sickafus, K. E.; Wills, J. M.; Grimes, N. W.: *J. Am. Chem. Soc.* **82** (1999) 3279-3292.

[12] Zhang, M.; de Respinis, M.; Frei, H.: *Nat. Chem.* **6** (2014) 362-367.

[13] Man, I. C.; Su, H.-Y.; Calle-Vallejo, F.; Hansen, H. A.; Martínez, J. I.; Inoglu, N. G.; Kitchin, J.; Jaramillo, T. F.;

Nørskov, J. K.; Rossmeisl, J.: *Chem. Cat. Chem.* **3** (2011) 1159-1165.

[14] Tung, C.-W.; Hsu, Y.-Y.; Shen, Y.-P.; Zheng, Y.; Chan, T.-S.; Sheu, H.-S.; Cheng, Y.-C.; Chen, H. M.: *Nat. Comm.* **6** (2015) 8106.

[15] Trotochaud, L.; Ranney, J. K.; Williams, K. N.; Boettcher, S. W.: *J. Am. Chem. Soc.* **134** (2012) 17253-17261.

[16] Butel, M.; Gautier, L.; Delmas, C.: *Solid State Ionics* **122** (1999) 271-284.

[17] Subbaraman, R.; Tripkovic, D.; Chang, K. C.; Strmcnik, D.; Paulikas, A. P.; Hirunsit, P.; Chan, M.; Greeley, J.; Stamenkovic, V.; Markovic, N. M.: *Nat. Mater.* **11** (2012) 550-557.

[18] Wang, H. Y.; Hsu, Y. Y.; Chen, R.; Chan, T. S.; Chen, H. M.; Liu, B.: *Adv. Energy Mater.* **5** (2015) 1500091.

[19] Wang, H.-Y.; Hung, S.-F.; Chen, H.-Y.; Chan, T.-S.; Chen, H. M.; Liu, B.: *J. Am. Chem. Soc.* **138** (2016) 36-39.

[20] Szotek, Z.; Temmerman, W. M.; Ködderitzsch, D.; Svane, A.; Petit, L.; Winter, H.: *Phys. Rev. B* **74** (2006) 174431.

[21] Van der Ven, A.; Morgan, D.; Meng, Y. S.; Ceder, G.: *J. Electro. Soc.* **153** (2006) A210-A215.

[22] Hsu, C. S.; Suen, N. T.; Hsu, Y. Y.; Lin, H. Y.; Tung, C. W.; Liao, Y. F.; Chan, T. S.; Sheu, H. S.; Chen, S. Y.; Chen, H. M.: *Phys Chem Chem Phys* **19** (2017) 8681-8693.